

nnMobileNet++: Towards Efficient Hybrid Networks for Retinal Image Analysis

Xin Li
Arizona State University
x.li@asu.edu

Hao Wang
Clemson University
hao9@g.clemson.edu

Wenhui Zhu
Arizona State University
wzhu59@asu.edu

Yujian Xiong
Arizona State University
yxiong42@asu.edu

Yalin Wang
Arizona State University
ylwang@asu.edu

Xuanzhao Dong
Arizona State University
xdong64@asu.edu

Oana M. Dumitrascu
Mayo Clinic
Dumitrascu.Oana@mayo.edu

Abstract

Retinal imaging is a critical, non-invasive modality for the early detection and monitoring of ocular and systemic diseases. Deep learning, particularly convolutional neural networks (CNNs), has significant progress in automated retinal analysis, supporting tasks such as fundus image classification, lesion detection, and vessel segmentation. As a representative lightweight network, nnMobileNet has demonstrated strong performance across multiple retinal benchmarks while remaining computationally efficient. However, purely convolutional architectures inherently struggle to capture long-range dependencies and model the irregular lesions and elongated vascular patterns that characterize on retinal images, despite the critical importance of vascular features for reliable clinical diagnosis. To further advance this line of work and extend the original vision of nnMobileNet, we propose nnMobileNet++, a hybrid architecture that progressively bridges convolutional and transformer representations. The framework integrates three key components: (i) dynamic snake convolution for boundary-aware feature extraction, (ii) stage-specific transformer blocks introduced after the second down-sampling stage for global context modeling, and (iii) retinal image pretraining to improve generalization. Experiments on multiple public retinal datasets for classification, together with ablation studies, demonstrate that nnMobileNet++ achieves state-of-the-art or highly competitive accuracy while maintaining low computational cost, underscoring its potential as a lightweight yet effective framework for retinal image analysis.

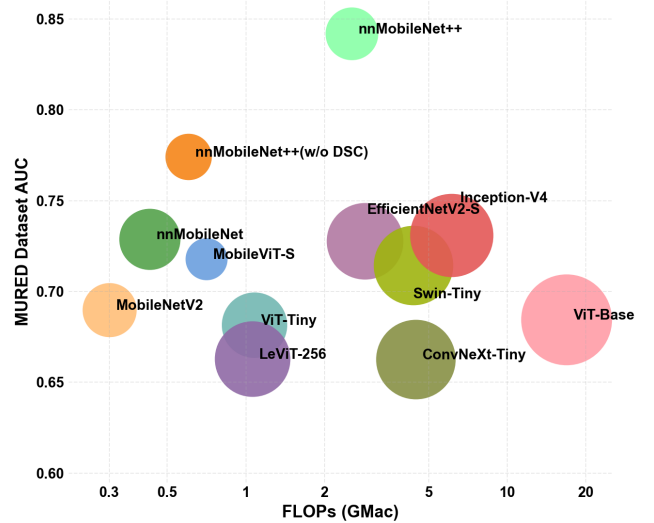


Figure 1. Comparison of FLOPs, parameter size, and AUC on the MURED dataset. Each bubble corresponds to a model, where the **bubble size** is proportional to the number of parameters, the **x-axis** indicates computational cost (FLOPs), and the **y-axis** shows classification performance (AUC). The nnMobileNet++ (w/o DSC) denotes the architecture after removing the Dynamic Snake Convolution module.

1. Introduction

Retinal imaging plays a critical role in modern medicine as a non-invasive and accessible modality for the early detection and longitudinal monitoring of ocular and systemic diseases [10, 50, 55, 59, 60]. Retinal disorders such as diabetic retinopathy, glaucoma, and age-related macular degeneration remain among the leading causes of visual im-

pairment and blindness worldwide, underscoring the urgent need for reliable diagnostic tools [6, 8, 9, 34, 43, 46, 47]. Beyond ophthalmology, retinal images also provide important biomarkers for systemic conditions including hypertension, diabetes, and neurodegenerative diseases such as Alzheimer’s disease, highlighting their broad clinical relevance [12–14]. In recent years, deep learning–based approaches have become the dominant paradigm for automated retinal image analysis, with convolution neural networks (CNNs) supporting tasks such as disease classification, lesion detection, and vessel segmentation [8–10, 14, 24, 47, 61, 61–63]. CNNs are effective for retinal image analysis using convolution operations extract features at the pixel level, enabling efficient detection of retinal structures such as lesions and vessels, while keeping the models sufficiently efficient for deployment on resource-constrained or edge devices [24, 40, 44, 62]. Among these efforts, nnMobileNet has emerged as a representative lightweight baseline, delivering competitive accuracy with low parameter counts and computational cost through a careful redesign of CNN components [62]. However, purely convolution architectures have limited ability to model long-range dependencies, which are essential for capturing the irregular lesions and spatially distributed vascular patterns commonly observed in retinal images. [11, 29, 32]

Vision Transformers (ViTs) have recently demonstrated notable capability in global context modeling across a range of computer vision benchmarks, effectively capturing long-range dependencies. In medical imaging, ViTs have been applied to tasks such as segmentation, organ delineation, and disease classification, showing steady progress [3, 11, 17, 24, 29, 32, 61]. For retinal analysis, global reasoning is particularly critical: Lesions often have irregular shapes and scattered spatial distribution, while vessels are thin and tortuous, and vascular characteristics are closely associated with ocular diseases and systemic conditions such as Alzheimer’s disease. These heterogeneous features require models to preserve fine boundary information while maintaining reliable global reasoning [5, 12, 14–16, 26, 27, 51, 57]. Nonetheless, routine application of ViTs in medical imaging remains constrained. Stable convergence often depends on large-scale, high-quality annotations, which are scarce and costly in clinical practice; moreover, the quadratic complexity of self-attention results in considerable computational and memory overhead, limiting deployment on resource-constrained diagnostic systems [11, 24, 29, 62]. These limitations motivate hybrid frameworks that retain the lightweight efficiency of CNNs while incorporating the contextual modeling strengths of ViTs. To further enhance vascular representation, we introduce Dynamic Snake Convolution (DSC) [37], enabling adaptive sampling along curvilinear structures. This helps preserve vessel continuity and morphology, and provides

structured features more effective in subsequent ViTs.

Motivated by the need to combine the efficiency of CNNs with the global dependency modeling of ViTs, we extend nnMobileNet [62] and propose nnMobileNet++, a hybrid framework that integrates local convolution representations with transformer-based global reasoning. This work makes the following key contributions: (i) an efficient hybrid architecture that integrates convolution and transformer components while maintaining lightweight design, (ii) the introduction of dynamic snake convolution [37] together with Vision Transformer modules before the Vision Transformer stage, which enhances boundary-sensitive local feature extraction and preserves curvilinear structures such as blood vessels during downsampling, and (iii) self-supervised pretraining on a large-scale retinal image dataset to enhance robustness and generalization. We evaluated the framework on multiple retinal image datasets, and the results demonstrate a favorable balance between accuracy and efficiency (Fig. 1), highlighting its practicality for retinal image analysis in clinical settings.

2. Related work

2.1. Lightweight CNN-Based Models

Lightweight CNNs have been widely adopted in retinal image analysis due to their efficiency and suitability for deployment on fundus cameras and edge devices [24, 30, 40, 44, 62]. Building on earlier models such as MobileNet [40] and EfficientNet [44], nnMobileNet [62] introduces task-specific refinements, including stage-wise channel allocation [19], heavy data augmentation strategies, AdamP optimization [22], spatial dropout, and ReLU6 activation [62]. These improvements enhance both accuracy and robustness across retinal benchmarks, while keeping computational demands low, establishing nnMobileNet as an efficient baseline. However, as a purely convolution model, nnMobileNet remains constrained in modeling long-range dependencies, which are essential for capturing complex retinal structures [11].

2.2. Transformer-Based and Hybrid Models

Vision Transformers (ViTs) were originally proposed as an alternative to convolution architectures, introducing self-attention mechanisms that enable explicit modeling of long-range dependencies and global context [11]. These strengths quickly led to widespread exploration in medical imaging, where ViTs have shown promising results in tasks such as organ segmentation, tumor delineation, and disease classification [4, 20, 52]. Nevertheless, standard ViT architectures require large annotated datasets to converge reliably and impose high computational and memory demands, which limit their adoption in clinical practice and on resource-constrained devices.

Hybrid architectures such as MobileViT [32] and LeViT [17] in the vision community have shown that combining convolution with lightweight attention can provide a good balance between accuracy and efficiency. While related ideas have also been explored in medical imaging, most existing designs were developed for generic benchmarks and lack adaptations to the structural characteristics of retinal images [3, 24]. Given nnMobileNet’s strong performance and lightweight design on retinal images [62], we adopt it as our baseline and incorporate Vision Transformer modules to enhance global dependency modeling.

2.3. Retinal-Specific Architectures

Retinal images present irregular lesions and thin, tortuous vessels that span large regions, with vascular morphology serving as a recognized biomarker for ocular and systemic diseases [5, 12, 15, 16, 26, 27, 48, 51, 53, 57]. While convolution neural networks (CNNs) are effective for local feature extraction, their limited receptive fields and downsampling can distort fine vascular structures. Vision Transformers (ViTs) naturally capture long-range dependencies and global context, making them well suited for distributed retinal features [11, 29, 31]. To preserve structural detail while retaining CNN efficiency, we incorporate dynamic snake convolution (DSC) [37] in the convolution stage. Standard convolutions use fixed kernels and often oversmooth or distort curved boundaries, whereas DSC is boundary-sensitive and adapts to curvilinear patterns [37]. This makes it particularly effective for modeling retinal vessels and irregular lesions, ensuring that such structures are preserved and passed to the ViT stage, where global dependencies can then be captured on top of reliable local features.

2.4. Self-Supervised Pretraining in Retinal Imaging

Medical imaging datasets are typically small, and labeled retinal data are especially limited due to the cost of expert annotation [23, 25, 62]. Self-supervised pretraining has emerged as an effective way to address this limitation and has shown benefits across modalities such as MRI, CT, and fundus photography [1, 14, 25, 45]. Within this line of work, generative masked image modeling has proven particularly suitable for medical imaging, as the reconstruction of missing regions encourages the network to capture both fine local details and broader structural patterns that are central to anatomical representation [18, 21, 56]. Building on this insight, we adopt SimMIM [56] for pretraining on large collections of unlabeled retinal data. Its design places no restrictions on network structure, making it well suited to our hybrid CNN–ViT framework and enabling the model to learn structural priors at multiple scales, thereby improving robustness and generalization across datasets.

3. Method

3.1. Overall Architecture

As illustrated in Fig. 2, we introduce nnMobileNet++, a four-stage hybrid network. The network begins with a stem convolution for low-level feature extraction, followed by four sequential stages. Stage 1 and Stage 2 retain the inverted residual linear bottleneck (IRLB) design of nnMobileNet [62], which use depthwise convolutions for spatial feature extraction and pointwise convolutions for channel mixing, achieving a trade-off between accuracy and efficiency [19, 62]. At the downsampling step of Stage 2, we introduce a Dynamic Snake Convolution (DSC) [37] to better preserve curvilinear retinal structures such as blood vessels before passing features into the transformer modules. Stage 3 and Stage 4 are built with Vision Transformer modules [11, 32], combining local convolutions with global self-attention to capture both fine-grained spatial details and long-range dependencies. Across the four stages, spatial resolution is reduced via IRLB-based downsampling, leading to a final downsampling factor of 32 relative to the input. Finally, a lightweight classification head aggregates hierarchical features for prediction. Importantly, nnMobileNet++ preserves the non-traditional but effective channel configuration [19] of nnMobileNet, as shown in Fig. 2(a). Overall, this design achieves a strong balance between efficiency and representational power, while retinal-specific pretraining further improves downstream task performance.

3.2. Dynamic Snake Convolution (DSC) for Vessel Structures

Standard convolution focuses on local neighborhoods, which can break vessel continuity—especially during downsampling [7, 37, 39]. To mitigate this, we adopt Dynamic Snake Convolution (DSC) [37], which adaptively models sampling offsets along curvilinear trajectories to better preserve vascular structure. Formally, the output at location x_0 is defined as:

$$y(x_0) = \sum_{i=1}^K w_i \cdot x(x_0 + p_i + \Delta p_i), \quad (1)$$

where K is the kernel size (number of sampling points), w_i are convolution weights, p_i are fixed grid locations, and Δp_i are learnable offsets predicted from the input.

Compared with other dynamic convolutions such as the deformable convolution [7], DSC models offset evolution along vessel-like paths, producing more stable alignment with elongated structures while remaining computationally tractable. Nevertheless, it introduces extra overhead. To balance accuracy and efficiency, we use DSC only once at the Stage 2 downsampling layer, based on three considerations. First, downsampling is where feature degradation

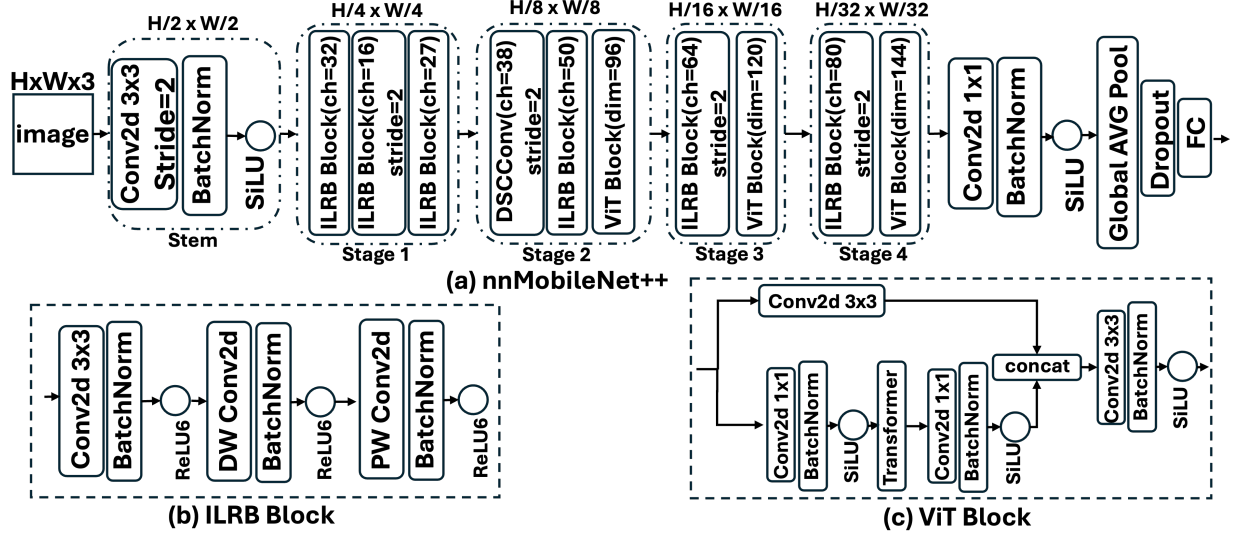


Figure 2. (a) Overall architecture of our network, consisting of four stages where early stages are CNN-based and later stages are ViT-based. At the second-stage downsampling, a **Dynamic Snake Convolution (DSC)** [37] is employed to better preserve curvilinear structures before feeding features into the ViTs. (b) The CNN blocks are built from nnMobileNet’s Inverted Residual Linear Bottleneck (IRLB), where **Depthwise (DW)** convolutions capture spatial information and **Pointwise (PW)** convolutions perform channel mixing. (c) The ViT modules combine local convolutions with global self-attention for contextual representation. “ch” denotes the number of input channels.

is most severe, making it the critical point for structural preservation [7, 37, 39]. Second, placing DSC at higher resolutions substantially increases computation [7]. Third, after the transition to Vision Transformers (ViTs), the features are reorganized into patch tokens and local continuity becomes less pertinent; consequently, the DSC module offers limited additional benefit in that stage [11, 29]. Accordingly, we apply a single DSC at the Stage 2 downsampling layer, right before passing the features into the ViT block. This design helps preserve vessel continuity at the stage where structural information is most likely to be lost, while at the same time avoiding the high computational cost of applying DSC at higher resolutions, and providing ViT with more coherent inputs for global modeling.

3.3. Vision Transformer Stage

In the ViT stage, we follow the MobileViT [32] design, where convolution is first applied for downsampling and local feature aggregation, and the resulting features are then processed by lightweight Transformer blocks for global dependency modeling, as shown in Fig. 2(c). Specifically, the input feature map $X \in \mathbb{R}^{H \times W \times C}$ is reduced to a compact representation $X' \in \mathbb{R}^{H' \times W' \times C'}$ via convolution, which is then projected into a sequence of tokens with positional encodings and fed into Transformer layers:

$$Z = \text{Transformer}(X'), \quad (2)$$

where each Transformer layer consists of Multi-Head Self-Attention (MHSA) and a Feed-Forward Network (FFN):

$$Z' = \text{FFN}(\text{MHSA}(Z)). \quad (3)$$

Finally, the outputs of the convolution and Transformer branches are fused before being passed to the subsequent stage. Concretely, a local projection is first applied on X and then added to Z' :

$$\hat{X} = \text{Conv}_{\text{local}}(X), \quad (4)$$

$$Y = \hat{X} + Z', \quad (5)$$

where Y denotes the fused feature map. This hybrid design enables convolution layers to capture fine local structures, while Transformer modules model long-range dependencies, together yielding representations that remain computationally compact while retaining strong descriptive capacity for retinal images.

3.4. Self-supervised Pretraining on Retinal Images

Self-supervised pretraining. To enhance generalization and stabilize optimization, we adopt masked image modeling for self-supervised pretraining. In particular, we use SimMIM [56], which reconstructs randomly masked regions from the visible context without requiring architectural changes, making it naturally compatible with our hybrid CNN-ViT network.

Formally, let $X \in \mathbb{R}^{H \times W \times C}$ be an input image and $M \in \{0, 1\}^{\tilde{H} \times \tilde{W}}$ a binary mask over patches (or pixels). Denote

the index set of masked locations by $\mathcal{I}_M = \{i \mid M_i = 1\}$. The model predicts the masked content \hat{X} , and the reconstruction loss is:

$$\mathcal{L}_{\text{SimMIM}} = \frac{1}{|\mathcal{I}_M|} \sum_{i \in \mathcal{I}_M} \|\hat{X}_i - X_i\|_1. \quad (6)$$

Here, i indexes a masked patch (or pixel); X_i and \hat{X}_i are the ground-truth and predicted RGB vectors for that location; $|\mathcal{I}_M|$ is the number of masked locations; and $\|\cdot\|_1$ is the L_1 (MAE) norm. Only masked positions contribute to the loss; visible regions are ignored.

Through this strategy, the model learns retinal vascular priors from large-scale unlabeled images and acquires more transferable representations, thereby improving downstream retinal analysis performance.

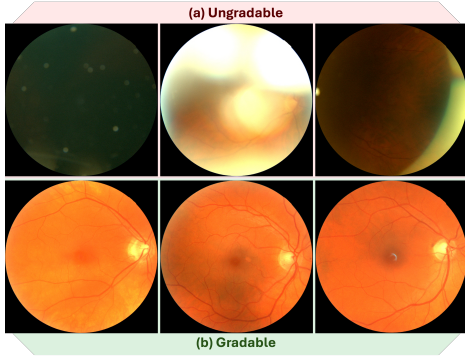


Figure 3. Examples of image quality in fundus images. The first row shows ungradable images excluded due to blur, poor illumination, or severe artifacts. The second row shows gradable images.

4. Experiments

4.1. Datasets

We evaluate nnMobileNet++ across six retinal datasets that span multi-label classification, multi-class categorization, and challenging MICCAI benchmarks involving ultra-widefield imaging and cross-device generalization.

UK Biobank [2]. For self-supervised pretraining, we use the UK Biobank, a large-scale cohort comprising 179,127 retinal color fundus photographs (CFPs). After applying the AutoMorph [58] pipeline for quality control, 114,275 gradable CFPs were retained. This large dataset provides sufficient diversity to learn robust retinal priors.

Multi-Label Retinal Diseases (MuReD) [38]. MuReD contains 2,208 CFPs (1,746 training and 444 test images). Each image is annotated with a 20-dimensional multi-hot label vector, covering 19 retinal disease categories plus an “other” class. This design allows multiple diseases to co-occur in one image, reflecting realistic clinical settings.

Ocular Disease Intelligent Recognition (ODIR) [42]. The ODIR dataset includes 7,000 CFPs from around 3,500 patients, annotated with eight disease categories: diabetes, glaucoma, cataract, age-related macular degeneration, hypertension, pathological myopia, other abnormalities, and normal. We follow the official DGCAHMO order and treat this as a multi-class disease classification task.

MICCAI 2023 Myopic Maculopathy Analysis Challenge (MMAC) [35]. The MMAC dataset provides 1,143 training and 248 validation images for grading myopic maculopathy severity into five levels, from tessellated fundus (grade 1) to macular atrophy (grade 4). This progression reflects increasing structural damage and offers a clinically meaningful benchmark for evaluating automated methods.

MICCAI 2024 Ultra-Widefield Fundus Imaging for Diabetic Retinopathy (UWF4DR) Challenge [36]. UWF4DR consists of three tasks: image quality assessment, referable diabetic retinopathy (DR) identification, and diabetic macular edema (DME) detection. Unlike conventional CFPs (30°–50° FoV), ultra-widefield (UWF) images capture up to 200° of the retina, making peripheral signs visible but also introducing peripheral distortion, uneven illumination, and greater anatomical variability.

MICCAI 2025 Multi-Camera Robust Diagnosis of Fundus Diseases (MuCaRD) [33]. MuCaRD includes 400 images with diabetic retinopathy and 400 with glaucoma. Since only the training set has been released, we adopt a 5-fold cross-validation protocol. The multi-camera acquisition setting introduces substantial variability in image quality and device characteristics, providing a stringent test of model robustness.

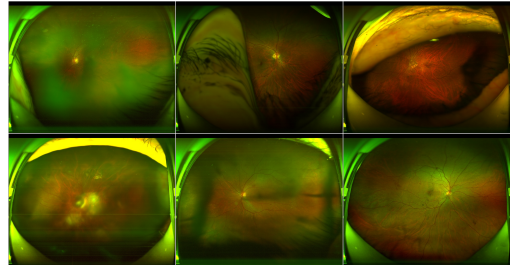


Figure 4. Examples of ultra-widefield (UWF) fundus images from the challenge dataset. The diversity of these images introduces challenges such as peripheral distortion, illumination non-uniformity, anatomical variability, and device/domain shifts.

4.2. Implementation Details

In both pretraining and classification tasks, input images were uniformly resized to 224×224 and trained with AdamW [49] optimizer (initial learning rate 1e-3, cosine decay schedule, and batch size 32), with standard normalization. Pretraining applied 60% random patch masking (patch size 32) and was run for 800 epochs with weight

Table 1. **Multi-Label Retinal Diseases (MuReD) dataset.** We report AUC, F1, and AUPRC; AUPRC is emphasized due to severe class imbalance. The right columns summarize computational cost and model size—*FLOPs (GMac)* and *Params (M)*—to assess deployability [28]. “Train from scratch” indicates models trained without external pretraining; “SSL” denotes self-supervised pretraining on retinal images for nnMobileNet++.

MIRel	AUC	F1	AUPRC	Train from scratch	FLOPs (GMac)	Params (M)
ConvNeXt-Tiny	0.663	0.063	0.136	Yes	4.455	27.801
EfficientNetV2-S	0.728	0.255	0.217	Yes	2.849	20.03
Inception-V4	0.731	0.196	0.204	Yes	6.123	41.087
LeViT	0.663	0.108	0.176	Yes	2.250	37.588
nnMobileNet	0.690	0.091	0.158	Yes	0.428	3.522
Swin Transformer-Tiny	0.714	0.218	0.244	Yes	4.371	27.500
ViT-Tiny	0.684	0.073	0.167	Yes	1.075	5.478
ViT-Base	0.682	0.053	0.173	Yes	16.848	85.612
MobileViT	0.718	0.123	0.188	Yes	1.420	4.929
MobileNetV2	0.690	0.091	0.158	Yes	0.3	2.196
nnMobileNet++*	0.805	0.334	0.335	Yes	2.538	2.1
nnMobileNet++	0.842	0.445	0.398	SSL	2.538	2.1

Table 2. **ODIR Dataset.** Results of multi-disease classification. We report AUC, F1, and Accuracy for baseline models and nnMobileNet++. nnMobileNet++* indicates training from scratch.

Model	AUC	F1	Accuracy
ConvNeXt	0.854	0.270	0.441
nnMobileNet	0.856	0.270	0.441
EfficientNetV2-S	0.855	0.270	0.441
Inception-V4	0.855	0.270	0.441
LeViT	0.859	0.272	0.442
MobileNetV2	0.869	0.304	0.449
MobileViT	0.868	0.288	0.448
Swin-Transformer	0.856	0.277	0.442
nnMobileNet++*	0.873	0.295	0.445
nnMobileNet++	0.906	0.494	0.536

decay 0.05 and 20 warmup epochs, using automatic mixed precision (AMP). For classification, all CNN and ViT baselines were trained from scratch using the timm library [54], while nnMobileNet++ was evaluated both from scratch and with a pretrained ReXNet backbone, trained for 300 epochs with weight decay $5e-4$. All experiments were implemented in PyTorch and executed on NVIDIA A100 GPUs(80GB).

4.3. Main Experiments

Multi-Label Classification Results. We evaluate a diverse set of CNN and ViT baselines alongside our proposed nnMobileNet++ on the MuRED dataset under a unified protocol. To ensure a fair comparison, all models are trained from scratch to isolate architectural capacity; we additionally perform self-supervised pretraining on retinal images to assess further gains on nnMobileNet++. As summarized in Table. 1, the scratch version of nnMobileNet++ obtains AUC 0.805 / F1 0.334 / AUPRC 0.335, outperform-

ing the strongest baselines (Inception-V4 for AUC 0.731, EfficientNetV2-S for F1 0.255, and Swin-Tiny for AUPRC 0.244) by +0.074 AUC / +0.079 F1 / +0.091 AUPRC. With self-supervised pretraining, nnMobileNet++ further improves to AUC 0.842 / F1 0.445 / AUPRC 0.398. In terms of efficiency, nnMobileNet++ requires only 2.5 GMacs FLOPs and 2.1M parameters, making it lightweight and suitable for deployment on resource-constrained devices; its FLOPs are substantially lower than mainstream ViT backbones such as Swin-Tiny (4.4 GMacs and 27.5M Parameters). These results indicate that the proposed architecture provides strong performance while remaining computationally compact, and that pretraining offers additional benefit in data-limited medical imaging scenarios.

Multi-Class Classification Results. On the ODIR dataset for multi-disease, multi-class retinal classification, baseline CNN and ViT models achieve AUC values around 0.85–0.87 but consistently suffer from very low F1 scores (≤ 0.304), highlighting the difficulty of multi-class prediction under class imbalance. As shown in Table. 2 Our nnMobileNet++ trained from scratch achieves an AUC of 0.873, F1 of 0.295, and Accuracy of 0.445, already matching or slightly surpassing the best baselines. With self-supervised pretraining and fine-tuning, nnMobileNet++ further improves to an AUC of 0.906, F1 of 0.494, and Accuracy of 0.536. This represents improvements of +0.033 AUC, +0.199 F1, and +0.091 Accuracy over its scratch counterpart, while substantially outperforming all baselines. These results indicate that nnMobileNet++ is highly effective for challenging multi-class, imbalanced retinal classification, and that self-supervised pretraining provides considerable additional benefit.

MICCAI Challenge Datasets Results. We further evaluate nnMobileNet++ on three recent MICCAI challenges, which provide clinically realistic and increasingly demand-

Table 3. **MICCAI 2024 UWF4DR dataset.** Results on ultra-widefield (UWF) fundus images, which present greater challenges due to peripheral distortion, illumination variability, and anatomical diversity. We evaluate three tasks: image quality assessment, diabetic retinopathy (DR) classification, and diabetic macular edema (DME) classification. Across all tasks, nnMobileNet++ achieves the best performance, consistently surpassing CNN and ViT baselines in terms of AUC, Accuracy, and F1.

Model	Image Quality Assessment			DR Classification			DME Classification		
	AUC	ACC	F1	AUC	ACC	F1	AUC	ACC	F1
ConvNeXt	0.846	0.787	0.787	0.762	0.680	0.680	0.775	0.644	0.644
EfficientNetV2-S	0.826	0.754	0.754	0.665	0.640	0.627	0.773	0.711	0.711
Inception-V4	0.840	0.738	0.738	0.770	0.740	0.740	0.807	0.756	0.751
LeViT	0.848	0.738	0.705	0.638	0.580	0.426	0.621	0.533	0.371
nnMobileNet	0.834	0.754	0.754	0.678	0.600	0.600	0.829	0.711	0.703
MobileNetV2	0.841	0.754	0.727	0.665	0.640	0.610	0.696	0.689	0.689
MobileViT	0.822	0.770	0.748	0.682	0.640	0.599	0.647	0.644	0.641
Swin-Transformer	0.703	0.607	0.607	0.716	0.580	0.580	0.666	0.600	0.600
ViT-Base	0.772	0.738	0.719	0.645	0.580	0.426	0.585	0.533	0.371
ViT-Tiny	0.824	0.787	0.763	0.623	0.580	0.426	0.587	0.600	0.589
nnMobileNet++	0.854	0.803	0.799	0.882	0.840	0.841	0.893	0.867	0.867

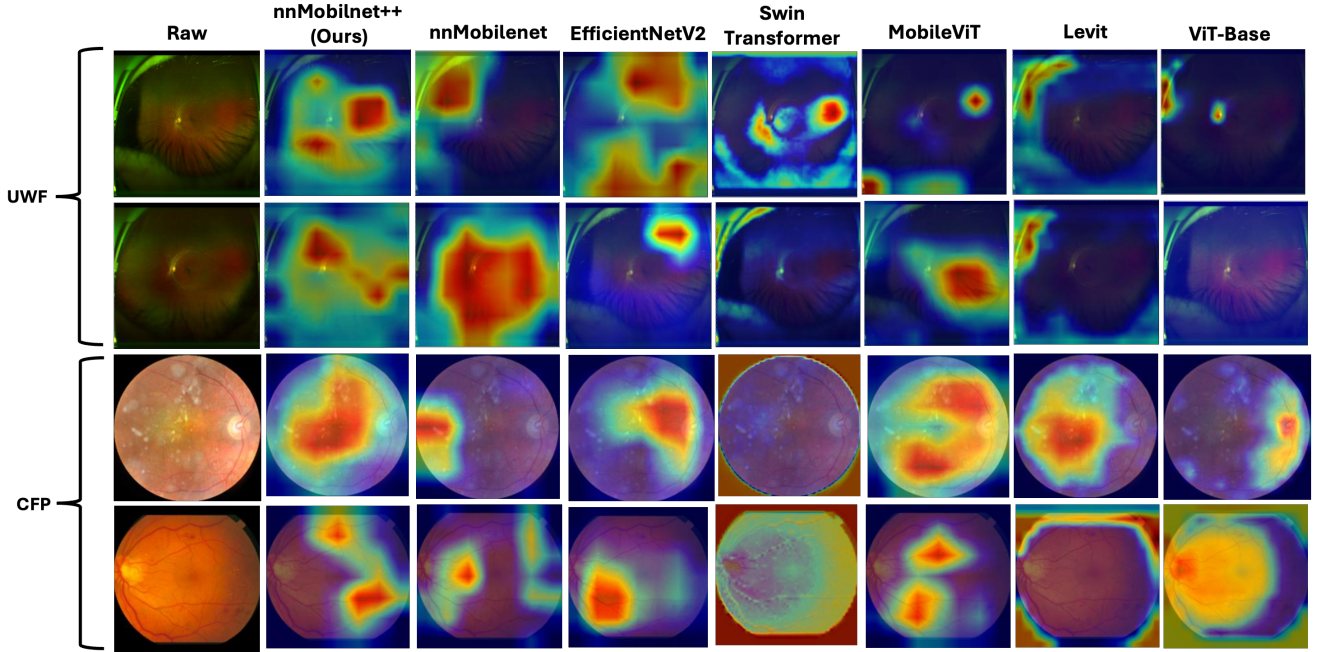


Figure 5. Class activation maps (CAMs) [41] generated by different networks. The first two rows show Ultra-Widefield Fundus Imaging (UWF) samples from the UWF4DR dataset, and the last two rows show color fundus photography (CFP) samples from the MURED dataset. Compared to existing baselines (nnMobilenet [62], EfficientNetV2 [44], Swin Transformer [29], MobileViT [32], LeViT [17], and ViT-Base [11]), our proposed nnMobileNet++ achieves consistently more accurate and focused attention on lesion regions across both UWF and CFP modalities.

ing benchmarks beyond standard fundus datasets. On **MMAC 2023**, which targets the grading of myopic maculopathy, disease progression is reflected in subtle morphological changes of the posterior pole that are often difficult for lightweight models to capture. As shown in Table 4, nnMobileNet++ achieves the best results (AUC 0.946 / F1

0.746 / Accuracy 0.758), demonstrating its capacity to capture fine-grained pathological variations more effectively than conventional CNN and ViT baselines. On **UWF4DR 2024**, which involves ultra-widefield (UWF) fundus images covering up to 200° of the retina [4], peripheral distortion, uneven illumination, and anatomical variability present major

Table 4. **MICCAI 2023 MMAC dataset.** We report AUC, F1, and Accuracy for various baseline models and nnMobileNet++.

Model	AUC	F1	Accuracy
ConvNeXt	0.572	0.513	0.513
EfficientNetV2-S	0.878	0.565	0.593
Inception-V4	0.783	0.411	0.448
MobileNetV2	0.855	0.554	0.585
MobileViT	0.878	0.588	0.621
Swin-Transformer	0.742	0.219	0.351
nnMobileNet	0.919	0.645	0.669
nnMobileNet++	0.946	0.746	0.758

Table 5. Ablation study conducted on the MICCAI MMAC 2023 dataset. *B*: nnMobileNet backbone; *V*: replacing the IRLB block with a ViT module; *S*: adding Dynamic Snake Conv (DSC) in place of the IRLB convolution; *P*: applying pretraining on retinal images. Performance is reported in terms of AUC, F1 score, FLOPs (GMac), and Params (M).

Index	<i>B</i>	<i>V</i>	<i>S</i>	<i>P</i>	AUC	F1	FLOPs	Params
1	✓	×	×	×	0.919	0.645	0.428	3.522
2	✓	✓	×	×	0.928	0.691	0.603	1.933
3	✓	✓	✓	×	0.935	0.730	2.538	2.100
4	✓	✓	✓	✓	0.946	0.746	2.538	2.100

Table 6. **MICCAI 2025 MuCaRD dataset.** This dataset is characterized by its multi-device acquisition setting. We report AUC, AUPRC, and F1 as evaluation metrics for baseline models and nnMobileNet++.

Model	AUC	AUPRC	F1
ConvNeXt	0.572	0.575	0.513
EfficientNetV2-S	0.629	0.630	0.513
Inception-V4	0.645	0.625	0.513
Swin-Transformer	0.598	0.601	0.513
LeViT	0.588	0.595	0.513
MobileNetV2	0.565	0.591	0.538
MobileViT	0.609	0.595	0.513
nnMobileNet	0.659	0.636	0.513
ViT-Tiny	0.563	0.561	0.513
ViT-Base	0.580	0.588	0.525
nnMobileNet++	0.739	0.725	0.669

challenges. As reported in Table 3, nnMobileNet++ consistently exceeds baselines in three tasks: image quality assessment, classification of diabetic retinopathy (DR), and classification of diabetic macular edema (DME). For example, it achieves an AUC of 0.893 and F1 of 0.867 on DME classification, confirming strong robustness to UWF-specific artifacts. On **MuCaRD 2025**, designed to as-

sess robustness across multiple imaging devices, substantial domain shifts in resolution, color, and illumination substantially degrade baseline performance. As shown in Table 6, nnMobileNet++ obtains the highest scores (AUC 0.739 / AUPRC 0.725 / F1 0.669), exceeding nnMobileNet by +0.080 AUC and +0.156 F1. These gains highlight its improved generalization under device heterogeneity, which is essential for real-world deployment. In summary, nnMobileNet++ achieves strong predictive performance while maintaining a lightweight design. It also shows robustness to disease heterogeneity, anatomical distortions, and device variability. This balance of accuracy and efficiency makes it well-suited for retinal image analysis in real-world clinical settings, especially under resource constraints.

4.4. Ablation Studies

We conduct ablation experiments on the **MICCAI MMAC 2023** dataset to assess the impact of each component in nnMobileNet++ (Table 5). Starting from the nnMobileNet backbone (AUC 0.919 / F1 0.645), replacing the IRLB block with a ViT module improves performance (AUC 0.928 / F1 0.691), confirming the value of global context modeling. Incorporating DSC further raises accuracy (AUC 0.935 / F1 0.730), demonstrating its effectiveness in maintaining vessel continuity. With pretraining, the model achieves the best results (AUC 0.946 / F1 0.746).

Overall, nnMobileNet++ enhances performance while reducing parameter count (3.5M \rightarrow 2.1M) and keeping FLOPs modest (≤ 2.5 GMacs). Importantly, the variant without DSC also performs competitively (AUC 0.928 / F1 0.691) with only 0.6 GMacs, showing that the framework remains highly efficient under tight computational budgets. We further validate this on the **MuReD** dataset (Fig. 1), where the variant without DSC but with pretraining still achieves strong AUC results. These findings indicate that nnMobileNet++ balances accuracy and efficiency, making it suitable for deployment across diverse environments.

4.5. Grad-CAM Visualization

Fig. 5 presents Grad-CAM [41] visualizations comparing nnMobileNet++ with several baselines. On the challenging UWF images (top two rows), nnMobileNet++ is still able to focus on lesion regions, whereas other models often fail to localize meaningful areas. On CFP images (bottom two rows), our model demonstrates superior precision, especially when lesions are small or visually subtle. For instance, in the last row, two faint DR lesions—likely corresponding to retinal hemorrhages or microaneurysms, which are difficult to detect due to their small size and color similarity to the surrounding retina—are correctly highlighted only by nnMobileNet++. Such visualizations are of great clinical importance, as they not only confirm the correctness of model predictions but also provide interpretability

for subtle and clinically relevant lesions.

5. Conclusion

We presented nnMobileNet++, a lightweight hybrid CNN–ViT framework enhanced with Dynamic Snake Convolution for retinal image analysis. Across MuReD, ODIR, and three MICCAI challenges, it consistently surpasses CNN and ViT baselines while remaining highly efficient. Grad-CAM visualizations confirm reliable localization of subtle lesions, supporting interpretability. These advances suggest nnMobileNet++ can provide accurate and scalable tools for retinal screening. Beyond technical performance, its efficiency and robustness make it particularly suited for integration into clinical research pipelines, where it may facilitate the discovery of imaging biomarkers and support precision medicine in ophthalmology and systemic disease.

References

- [1] Shekoofeh Azizi, Basil Mustafa, Fiona Ryan, Zachary Beaver, Jan Freyberg, Jonathan Deaton, Aaron Loh, Alan Karthikesalingam, Simon Kornblith, Ting Chen, et al. Big self-supervised models advance medical image classification. In *Proceedings of the IEEE/CVF international conference on computer vision*, pages 3478–3488, 2021. 3
- [2] Clare Bycroft, Colin Freeman, Desislava Petkova, Gavin Band, Lloyd T Elliott, Kevin Sharp, Allan Motyer, Damjan Vukcevic, Olivier Delaneau, Jared O’Connell, et al. The uk biobank resource with deep phenotyping and genomic data. *Nature*, 562(7726):203–209, 2018. 5
- [3] Hu Cao, Yueyue Wang, Joy Chen, Dongsheng Jiang, Xiaopeng Zhang, Qi Tian, and Manning Wang. Swin-unet: Unet-like pure transformer for medical image segmentation. In *European conference on computer vision*, pages 205–218. Springer, 2022. 2, 3
- [4] Jieneng Chen, Yongyi Lu, Qihang Yu, Xiangde Luo, Ehsan Adeli, Yan Wang, Le Lu, Alan L Yuille, and Yuyin Zhou. Transunet: Transformers make strong encoders for medical image segmentation. *arXiv preprint arXiv:2102.04306*, 2021. 2
- [5] Jacqueline Chua, Calvin Woon Loong Chin, Jimmy Hong, Miao Li Chee, Thu-Thao Le, Daniel Shu Wei Ting, Tien Yin Wong, and Leopold Schmetterer. Impact of hypertension on retinal capillary microvasculature using optical coherence tomographic angiography. *Journal of hypertension*, 37(3): 572–580, 2019. 2, 3
- [6] Nathan Congdon, Benita O’Colmain, CC Klaver, Ronald Klein, Beatriz Muñoz, David S Friedman, John Kempen, Hugh R Taylor, Paul Mitchell, et al. Causes and prevalence of visual impairment among adults in the united states. *Archives of Ophthalmology (Chicago, Ill.: 1960)*, 122(4): 477–485, 2004. 2
- [7] Jifeng Dai, Haozhi Qi, Yuwen Xiong, Yi Li, Guodong Zhang, Han Hu, and Yichen Wei. Deformable convolutional networks. In *Proceedings of the IEEE international conference on computer vision*, pages 764–773, 2017. 3, 4
- [8] Xuanzhao Dong, Yalin Wang, Yanxi Chen, Xin Li, Hao Wang, Peijie Qiu, Xiwen Chen, Abolfazl Razi, Yujian Xiong, Oana M Dumitrascu, et al. Dme-mobilenet: Fine-tuning nn-mobilenet for diabetic macular edema classification. In *MICCAI Challenge on Ultra-Widefield Fundus Imaging for Diabetic Retinopathy*, pages 155–164. Springer, 2024. 2
- [9] Xuanzhao Dong, Vamsi Krishna Vasa, Wenhui Zhu, Peijie Qiu, Xiwen Chen, Yi Su, Yujian Xiong, Zhangsihao Yang, Yanxi Chen, and Yalin Wang. Cunsb-rfie: Context-aware unpaired neural schrödinger bridge in retinal fundus image enhancement. In *2025 IEEE/CVF Winter Conference on Applications of Computer Vision (WACV)*, pages 4502–4511. IEEE, 2025. 2
- [10] Xuanzhao Dong, Wenhui Zhu, Xin Li, Guoxin Sun, Yi Su, Oana M Dumitrascu, and Yalin Wang. Tpot: Topology preserving optimal transport in retinal fundus image enhancement. In *2025 IEEE 22nd International Symposium on Biomedical Imaging (ISBI)*, pages 1–5. IEEE, 2025. 1, 2
- [11] Alexey Dosovitskiy, Lucas Beyer, Alexander Kolesnikov, Dirk Weissenborn, Xiaohua Zhai, Thomas Unterthiner, Mostafa Dehghani, Matthias Minderer, Georg Heigold, Sylvain Gelly, et al. An image is worth 16x16 words: Transformers for image recognition at scale. *arXiv preprint arXiv:2010.11929*, 2020. 2, 3, 4, 7
- [12] Oana M Dumitrascu, Bart M Demaerschalk, Cristina Valencia Sanchez, Diana Almader-Douglas, Cumara B O’Carroll, Maria I Aguilar, Patrick D Lyden, and Gyanendra Kumar. Retinal microvascular abnormalities as surrogate markers of cerebrovascular ischemic disease: a meta-analysis. *Journal of Stroke and Cerebrovascular Diseases*, 27(7):1960–1968, 2018. 2, 3
- [13] Oana M. Dumitrascu, Xin Li, Wenhui Zhu, Bryan K. Woodruff, Simona Nikolova, Jacob Sobczak, Amal Youssef, Siddhant Saxena, Janine Andreev, Richard J. Caselli, John J. Chen, and Yalin Wang. Color fundus photography and deep learning applications in alzheimer disease. *Mayo Clinic Proceedings: Digital Health*, 2(4):548–558, 2024.
- [14] Oana M Dumitrascu, Xin Li, Wenhui Zhu, Bryan K Woodruff, Simona Nikolova, Jacob Sobczak, Amal Youssef, Siddhant Saxena, Janine Andreev, Richard J Caselli, et al. Color fundus photography and deep learning applications in alzheimer disease. *Mayo Clinic Proceedings: Digital Health*, 2(4):548–558, 2024. 2, 3
- [15] Fariztah Sukainah Nur Fathimah, Sauli Ari Widjaja, Wimbo Sasono, Ima Yustiarini, Muhammad Firmansjah, Ady Dwi Prakosa, Aulia Kezia Mulyazhara, and Soebagijo Adi Soelistijo. Retinal vessel tortuosity and fractal dimension in diabetic retinopathy. *International Journal of Retina and Vitreous*, 11(1):64, 2025. 3
- [16] Shawn Frost, Yogi Kanagasingam, Hamid Sohrabi, Janardhan Vignarajan, Pierrick Bourgeat, Oliver Salvado, Victor Villemagne, Christopher C Rowe, S Lance MacAulay, Cassandra Szoek, et al. Retinal vascular biomarkers for early detection and monitoring of alzheimer’s disease. *Translational psychiatry*, 3(2):e233–e233, 2013. 2, 3
- [17] Benjamin Graham, Alaaeldin El-Nouby, Hugo Touvron, Pierre Stock, Armand Joulin, Hervé Jégou, and Matthijs Douze. Levit: a vision transformer in convnet’s clothing for

- faster inference. In *Proceedings of the IEEE/CVF international conference on computer vision*, pages 12259–12269, 2021. 2, 3, 7
- [18] Anubhav Gupta, Islam Osman, Mohamed S Shehata, and John W Braun. Medmae: A self-supervised backbone for medical imaging tasks. *arXiv preprint arXiv:2407.14784*, 2024. 3
- [19] Dongyoon Han, Sangdoo Yun, Byeongho Heo, and YoungJoon Yoo. Rethinking channel dimensions for efficient model design. In *Proceedings of the IEEE/CVF conference on Computer Vision and Pattern Recognition*, pages 732–741, 2021. 2, 3
- [20] Ali Hatamizadeh, Yucheng Tang, Vishwesh Nath, Dong Yang, Andriy Myronenko, Bennett Landman, Holger R Roth, and Daguang Xu. Unetr: Transformers for 3d medical image segmentation. In *Proceedings of the IEEE/CVF winter conference on applications of computer vision*, pages 574–584, 2022. 2
- [21] Kaiming He, Xinlei Chen, Saining Xie, Yanghao Li, Piotr Dollár, and Ross Girshick. Masked autoencoders are scalable vision learners. In *Proceedings of the IEEE/CVF conference on computer vision and pattern recognition*, pages 16000–16009, 2022. 3
- [22] Byeongho Heo, Sanghyuk Chun, Seong Joon Oh, Dongyoon Han, Sangdoo Yun, Gyuwan Kim, Youngjung Uh, and Jung-Woo Ha. Adampt: Slowing down the slowdown for momentum optimizers on scale-invariant weights. *arXiv preprint arXiv:2006.08217*, 2020. 2
- [23] Álvaro S Hervella, José Rouco, Jorge Novo, and Marcos Ortega. Learning the retinal anatomy from scarce annotated data using self-supervised multimodal reconstruction. *Applied Soft Computing*, 91:106210, 2020. 3
- [24] Xin Li, Wenhui Zhu, Xuanzhao Dong, Oana M Dumitrascu, and Yalin Wang. Evit-unet: U-net like efficient vision transformer for medical image segmentation on mobile and edge devices. In *2025 IEEE 22nd International Symposium on Biomedical Imaging (ISBI)*, pages 1–5. IEEE, 2025. 2, 3
- [25] Xin Li, Wenhui Zhu, Peijie Qiu, Oana M Dumitrascu, Amal Youssef, and Yalin Wang. A bert-style self-supervised learning cnn for disease identification from retinal images. *arXiv preprint arXiv:2504.18049*, 2025. 3
- [26] Laurence S Lim, Miao Li Chee, Carol Y Cheung, and Tien Yin Wong. Retinal vessel geometry and the incidence and progression of diabetic retinopathy. *Investigative ophthalmology & visual science*, 58(6):BIO200–BIO205, 2017. 2, 3
- [27] Shuai Liu, Lei Liu, Cuixia Ma, Shu Su, Ying Liu, and Bin Li. Association between retinal vascular fractal dimensions and retinopathy of prematurity: an ai-assisted retrospective case-control study. *International Ophthalmology*, 45(1):1–11, 2025. 2, 3
- [28] Zhengdong Liu and contributors. Thop: Pytorch-opcounter. <https://github.com/Lyken17/pytorch-OpCounter>, 2019. 6
- [29] Ze Liu, Yutong Lin, Yue Cao, Han Hu, Yixuan Wei, Zheng Zhang, Stephen Lin, and Baining Guo. Swin transformer: Hierarchical vision transformer using shifted windows. In *Proceedings of the IEEE/CVF international conference on computer vision*, pages 10012–10022, 2021. 2, 3, 4, 7
- [30] Zhuang Liu, Hanzi Mao, Chao-Yuan Wu, Christoph Feichtenhofer, Trevor Darrell, and Saining Xie. A convnet for the 2020s. In *Proceedings of the IEEE/CVF conference on computer vision and pattern recognition*, pages 11976–11986, 2022. 2
- [31] Wenjie Luo, Yujia Li, Raquel Urtasun, and Richard Zemel. Understanding the effective receptive field in deep convolutional neural networks. *Advances in neural information processing systems*, 29, 2016. 3
- [32] Sachin Mehta and Mohammad Rastegari. Mobilevit: lightweight, general-purpose, and mobile-friendly vision transformer. *arXiv preprint arXiv:2110.02178*, 2021. 2, 3, 4, 7
- [33] MICCAI. Multi-camera robust diagnosis of fundus diseases (mucard) challenge, miccai 2025. Zenodo, 2025. 5
- [34] World Health Organization. *Prevention of blindness from diabetes mellitus: report of a WHO consultation in Geneva, Switzerland, 9-11 November 2005*. World Health Organization, 2006. 2
- [35] MMAC 2023 Organizers. Miccai mmac 2023 - myopic maculopathy analysis challenge. <https://codalab.lisn.upsaclay.fr/competitions/12477>, 2023. Accessed: 2025-09-15. 5
- [36] UWF4DR Organizers. Miccai uwf4dr 2024 - ultra-widefield fundus imaging for diabetic retinopathy challenge. <https://codalab.lisn.upsaclay.fr/competitions/18605>, 2024. Accessed: 2025-09-15. 5
- [37] Yaolei Qi, Yuting He, Xiaoming Qi, Yuan Zhang, and Guanyu Yang. Dynamic snake convolution based on topological geometric constraints for tubular structure segmentation. In *Proceedings of the IEEE/CVF international conference on computer vision*, pages 6070–6079, 2023. 2, 3, 4
- [38] Manuel Alejandro Rodriguez Rivera, Hasan Al-Marzouqi, and Panos Liatsis. Multi-label retinal diseases (mured) dataset. Kaggle dataset, 2022. 5
- [39] Olaf Ronneberger, Philipp Fischer, and Thomas Brox. U-net: Convolutional networks for biomedical image segmentation. In *International Conference on Medical image computing and computer-assisted intervention*, pages 234–241. Springer, 2015. 3, 4
- [40] Mark Sandler, Andrew Howard, Menglong Zhu, Andrey Zhmoginov, and Liang-Chieh Chen. Mobilenetv2: Inverted residuals and linear bottlenecks. In *Proceedings of the IEEE conference on computer vision and pattern recognition*, pages 4510–4520, 2018. 2
- [41] Ramprasaath R Selvaraju, Michael Cogswell, Abhishek Das, Ramakrishna Vedantam, Devi Parikh, and Dhruv Batra. Grad-cam: Visual explanations from deep networks via gradient-based localization. In *Proceedings of the IEEE international conference on computer vision*, pages 618–626, 2017. 7, 8
- [42] Ltd. Shangong Medical Technology Co. Ocular disease intelligent recognition (odir) dataset. <https://www.kaggle.com/datasets/andrewmvd/ocular-disease-recognition-odir5k>, 2019. Accessed: 2025-09-15. 5

- [43] Jaimie D Steinmetz, Rupert RA Bourne, Paul Svitil Briant, Seth R Flaxman, Hugh RB Taylor, Jost B Jonas, Amir Aberhe Abdoli, Woldu Aberhe Abrha, Ahmed Abualhasan, Eman Girum Abu-Gharbieh, et al. Causes of blindness and vision impairment in 2020 and trends over 30 years, and prevalence of avoidable blindness in relation to vision 2020: the right to sight: an analysis for the global burden of disease study. *The Lancet Global Health*, 9(2):e144–e160, 2021. 2
- [44] Mingxing Tan and Quoc Le. Efficientnet: Rethinking model scaling for convolutional neural networks. In *International conference on machine learning*, pages 6105–6114. PMLR, 2019. 2, 7
- [45] Yucheng Tang, Dong Yang, Wenqi Li, Holger R Roth, Bennett Landman, Daguang Xu, Vishwesh Nath, and Ali Hatamizadeh. Self-supervised pre-training of swin transformers for 3d medical image analysis. In *Proceedings of the IEEE/CVF conference on computer vision and pattern recognition*, pages 20730–20740, 2022. 3
- [46] Vamsi Krishna Vasa, Peijie Qiu, Wenhui Zhu, Yujian Xiong, Oana Dumitrascu, and Yalin Wang. Context-aware optimal transport learning for retinal fundus image enhancement. In *2025 IEEE/CVF Winter Conference on Applications of Computer Vision (WACV)*, pages 4016–4025. IEEE, 2025. 2
- [47] Hao Wang, Wenhui Zhu, Xuanzhao Dong, Yanxi Chen, Xin Li, Peijie Qiu, Xiwen Chen, Vamsi Krishna Vasa, Yujian Xiong, Oana M Dumitrascu, et al. Many-mobilenet: Multi-model augmentation for robust retinal disease classification. In *MICCAI Challenge on Ultra-Widefield Fundus Imaging for Diabetic Retinopathy*, pages 144–154. Springer, 2024. 2
- [48] Hao Wang, Wenhui Zhu, Jiayou Qin, Xin Li, Oana Dumitrascu, Xiwen Chen, Peijie Qiu, Abolfazl Razi, and Yalin Wang. Rbad: A dataset and benchmark for retinal vessels branching angle detection. In *2024 IEEE EMBS International Conference on Biomedical and Health Informatics (BHI)*, pages 1–8. IEEE, 2024. 3
- [49] Hang Wang, Xin Ye, Feng Tao, Chenbin Pan, Abhirup Mallik, Burhaneddin Yaman, Liu Ren, and Junshan Zhang. Adawm: Adaptive world model based planning for autonomous driving. *arXiv preprint arXiv:2501.13072*, 2025. 5
- [50] Jinyuan Wang, Ya Xing Wang, Dian Zeng, Zhuoting Zhu, Dawei Li, Yuchen Liu, Bin Sheng, Andrzej Grzybowski, and Tien Yin Wong. Artificial intelligence-enhanced retinal imaging as a biomarker for systemic diseases. *Theranostics*, 15(8):3223, 2025. 1
- [51] Le Wang, Jun-Yi Wang, Cheng Chen, Min Kang, San-Hua Xu, Hong Wei, Qian Ling, Liang-Qi He, Jie Zou, Xu Chen, et al. Octa evaluates changes in retinal microvasculature in renal hypertension patients. *Scientific Reports*, 14(1):28910, 2024. 2, 3
- [52] Wenxuan Wang, Chen Chen, Meng Ding, Hong Yu, Sen Zha, and Jiangyun Li. Transbts: Multimodal brain tumor segmentation using transformer. In *International conference on medical image computing and computer-assisted intervention*, pages 109–119. Springer, 2021. 2
- [53] Xinyu Wang, Hui Zhang, Hui Lu, Baixue Zhang, Bo Li, and Lifan Gao. Retinal microangiopathy as a marker of coronary atherosclerotic heart disease. *International Journal of General Medicine*, pages 4181–4193, 2025. 3
- [54] Ross Wightman. Pytorch image models. <https://github.com/rwightman/pytorch-image-models>, 2019. 6
- [55] Risa M Wolf, Roomasa Channa, Michael D Abramoff, and Harold P Lehmann. Cost-effectiveness of autonomous point-of-care diabetic retinopathy screening for pediatric patients with diabetes. *JAMA ophthalmology*, 138(10):1063–1069, 2020. 1
- [56] Zhenda Xie, Zheng Zhang, Yue Cao, Yutong Lin, Jianmin Bao, Zhuliang Yao, Qi Dai, and Han Hu. Simmim: A simple framework for masked image modeling. In *Proceedings of the IEEE/CVF conference on computer vision and pattern recognition*, pages 9653–9663, 2022. 3, 4
- [57] Shijia Zhou, Qifeng Yan, Jiaqi Guo, Wenming He, and Yitian Zhao. Early diagnosis of coronary heart disease based on retinal microvascular parameters of octa. *Frontiers in Cell and Developmental Biology*, 13:1654159, 2025. 2, 3
- [58] Yukun Zhou, Siegfried K Wagner, Mark A Chia, An Zhao, Moucheng Xu, Robbert Struyven, Daniel C Alexander, Pearse A Keane, et al. Automorph: automated retinal vascular morphology quantification via a deep learning pipeline. *Translational vision science & technology*, 11(7):12–12, 2022. 5
- [59] Wenhui Zhu, Peijie Qiu, Oana M Dumitrascu, Jacob M Sobczak, Mohammad Farazi, Zhangsihao Yang, Keshav Nandakumar, and Yalin Wang. Otre: Where optimal transport guided unpaired image-to-image translation meets regularization by enhancing. In *International Conference on Information Processing in Medical Imaging*, pages 415–427. Springer, 2023. 1
- [60] Wenhui Zhu, Peijie Qiu, Mohammad Farazi, Keshav Nandakumar, Oana M Dumitrascu, and Yalin Wang. Optimal transport guided unsupervised learning for enhancing low-quality retinal images. In *2023 IEEE 20th International Symposium on Biomedical Imaging (ISBI)*, pages 1–5. IEEE, 2023. 1
- [61] Wenhui Zhu, Xiwen Chen, Peijie Qiu, Mohammad Farazi, Aristeidis Sotiras, Abolfazl Razi, and Yalin Wang. Selfreg-net: Self-regularized unet for medical image segmentation. In *International Conference on Medical Image Computing and Computer-Assisted Intervention*, pages 601–611. Springer, 2024. 2
- [62] Wenhui Zhu, Peijie Qiu, Xiwen Chen, Xin Li, Natasha Lepore, Oana M Dumitrascu, and Yalin Wang. nnmobilenet: rethinking cnn for retinopathy research. In *Proceedings of the IEEE/CVF Conference on Computer Vision and Pattern Recognition*, pages 2285–2294, 2024. 2, 3, 7
- [63] Wenhui Zhu, Xin Li, Xiwen Chen, Peijie Qiu, Vamsi Krishna Vasa, Xuanzhao Dong, Yanxi Chen, Natasha Lepore, Oana Dumitrascu, Yi Su, et al. Retinalgpt: A retinal clinical preference conversational assistant powered by large vision-language models. *arXiv preprint arXiv:2503.03987*, 2025. 2